Ground Support 2026 - D Cumming-Potvin & J Wesseloo (eds.)
© 2026 Australian Centre for Geomechanics, Perth
doi:10.36487/ACG_repo/2625_31

Energy-absorbing rockbolt behaviour under combination loading angle configurations

John Hadjigeorgiou [a,*], Greig Knox [b]

[a] *University of Toronto, Canada*

[b] *Epiroc, South Africa*

Abstract

Energy-absorbing rockbolts are applied in ground conditions where large deformations are anticipated. In such conditions, it is expected that the rockbolt may be subjected to multiple loading configurations ranging from axial through to shear. The relationship between the loading angle and energy capacity of a rockbolt represents a knowledge gap that may account for the difference in performance observed in the field and recorded in the laboratory testing.

This paper investigates the mechanical behaviour of energy-absorbing rockbolts under quasi-static loading for a range of loading angles. A combination shear and tensile pull test rig was employed to simulate axial (0°) combination shear and loading with resultant loading angles (30 and 60°) and shear loading (90°) All selected rockbolts employed the 'steel stretching' mechanism whereby energy is dissipated through the plastic deformation of the bar between two anchor points bounding the loaded section. This includes paddled energy-absorbing, yielding mechanical hybrid and energy-absorbing self-drilling rockbolt types.

The results identified variations in performance as a function of loading angle for all rockbolt types. In addition, the presence or absence of a chemical anchoring medium was identified as a critical factor in the response of the rockbolts to combination loading. The results provide the means for a data driven design approach recognising difference in behaviour of energy-absorption rockbolts under complex loading quasi-static loading conditions.

Keywords: *energy-absorbing rockbolts, quasi-static loading, combined loading configurations, steel stretching mechanism*

1 Introduction

During the last 20 years, energy-absorbing rockbolts have become an integral part of ground support strategies in seismic and squeezing ground conditions. Although it is readily conceded that they perform better than conventional rockbolts, their performance under multiple loading configurations is not well defined. This is due to the difficulties in implementing controlled testing to quantify the rockbolt response under complex loading conditions. The majority of quasi-static tests simulate axial (0°) loading with limited shear loading (90°) tests (Knox & Hadjigeorgiou 2025). The exceptions is the work of Chen & Li (2015) and Knox & Hadjigeorgiou (2024a) who investigated multiple loading angle configurations for paddled energy-absorbing rockbolts. Drop tests are routinely used to determine the energy capacity of rockbolts but all tests are almost exclusively axial (Li et al. 2021).

This paper investigates the mechanical behaviour of energy-absorbing rockbolts under quasi-static loading for a range of loading angles. To these purposes, a combination shear and tensile pull test rig was employed

* Corresponding author. Email address: John.Hadjigeorgiou@utoronto.ca

to simulate axial (0°), combination shear and loading with resultant loading angles (30 and 60°) and shear loading (90°).

2 Energy-absorbing rockbolts

Although there are multiple energy-absorbing rockbolts commercially available, the most popular types employ 'steel stretching' where energy is dissipated through the plastic deformation of the bar between 2 anchor points bounding the loaded section. The mechanical properties and geometry of the tendon govern the performance of the rockbolt.

Figure 1 illustrates the 3 types of energy-absorbing rockbolts used in this study. The base component of the paddled energy-absorbing rockbolt (PEAR) (Li 2010) is the steel bar into which one or more paddle sets and a threaded length are formed (Figure 1a). The 'free length' between the paddles sets or a paddle set, and the threaded portion is debonded from the anchoring medium (resin or cementitious grout) when a load is applied. The energy is dissipated through the plastic deformation of the steel bar between the paddle sets or threaded anchor bounding the joint or bulking rock mass. Figure 1b illustrates the yielding mechanical hybrid rockbolt (YMHR) consisting of a steel tendon mechanically anchored within a friction bolt is percussion driven by the rockdrill and the mechanical anchor is subsequently activated using rotation (Knox & Hadjigeorgiou 2022). Figure 1c is a typical self-drilling yielding hollow rockbolt (SDYHR) which has sacrificial drill bit attached to the threaded anchor (Knox & Hadjigeorgiou 2023b). The yielding mechanism is achieved when the smooth hollow bar between the threaded anchor sections decouples from the grouting medium and elongates when load is applied to the rockbolt.

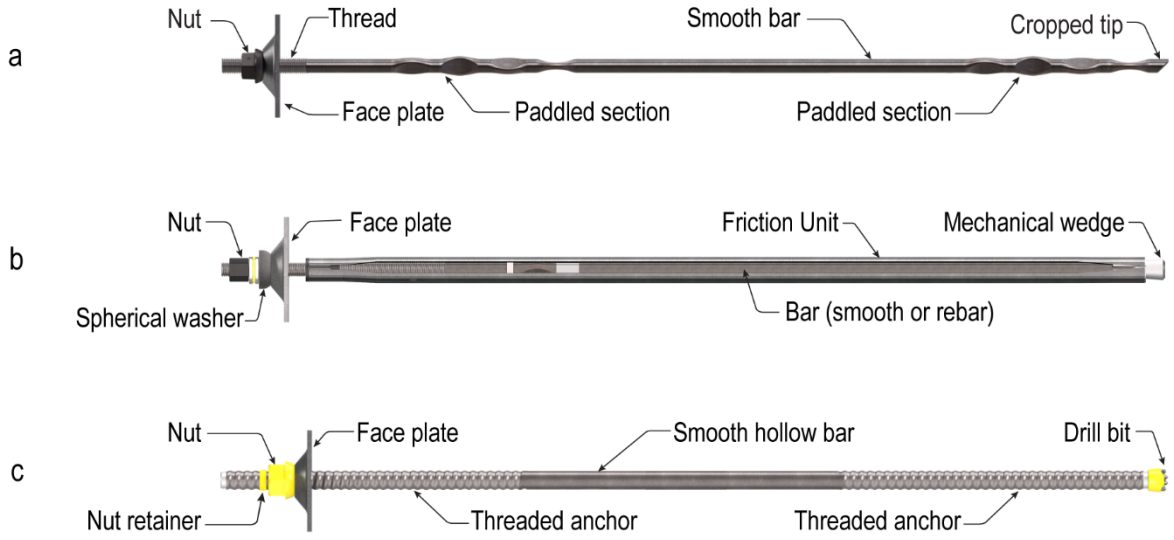


Figure 1 (a) Paddled energy-absorbing rockbolt; (b) Yielding mechanical hybrid rockbolt; (c) Yielding hollow rockbolt

The use of YMHR and SDYHR are of interest in heavily fractured and/or highly stressed rock, where the installation of rockbolts can be problematic due to hole closures and blown-out holes. Both rockbolt types can potentially overcome installation issues associated with resin penetration into fractures in the surrounding rock mass.

3 Experimental set up

The schematic of the testing configuration for combined loading is illustrated in Figure 2, and the sample preparation and material properties are described in detail in Knox & Hadjigeorgiou (2023a). The same apparatus was used for the in all tests for the PEARs, the YMHRs and the yielding hollow rockbolts.

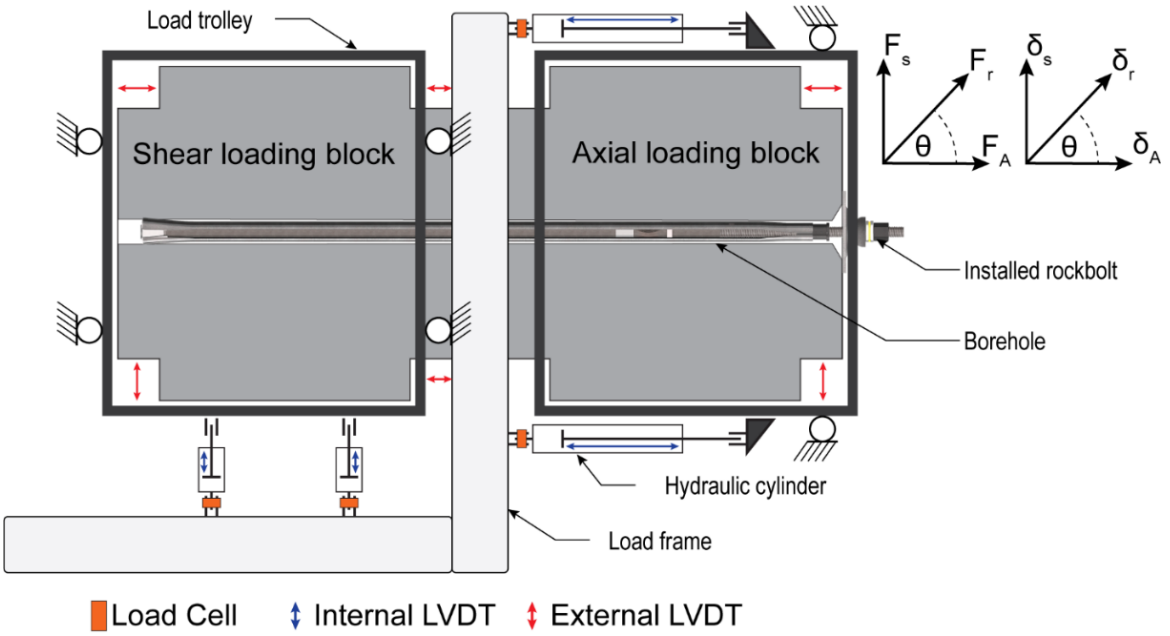


Figure 2 Schematic of the Epiroc combination shear tensile rockbolt pull tester (Knox & Hadjigeorgiou 2024b)

All 3 types of rockbolts were tested under axial (0°), combination (30 and 60°) or shear (90°) loading configurations. The loading angle is referenced relative from the axis of the borehole as illustrated in Figure 3 and the testing configuration for PEARs is shown in Figure 4. Similar setups were used for YMHRs and yielding hollow rockbolts.

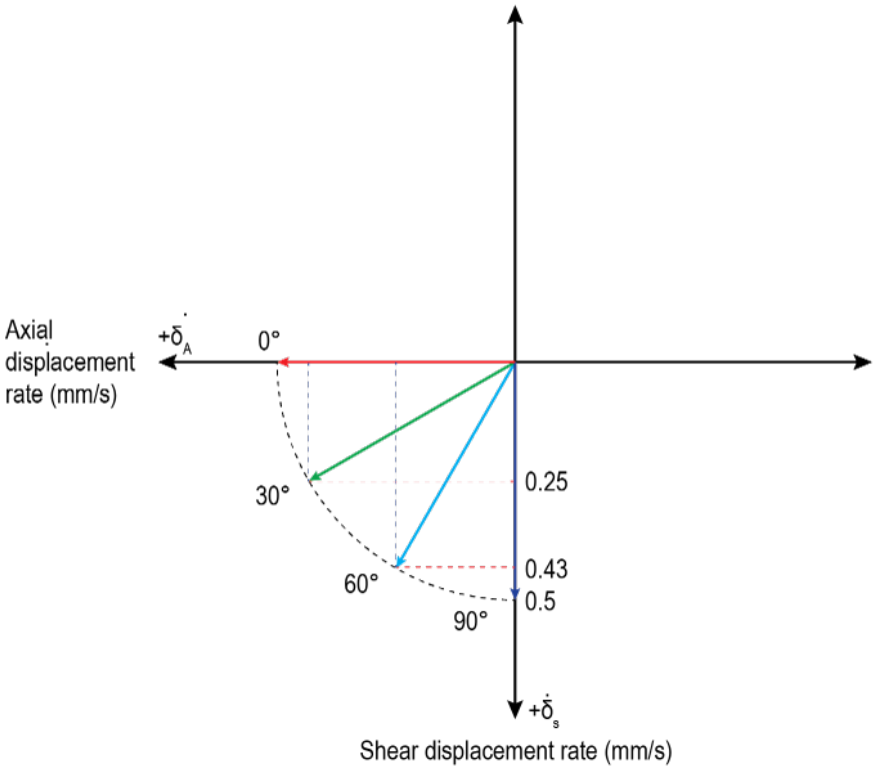


Figure 3 Illustration of the loading coordinates convention

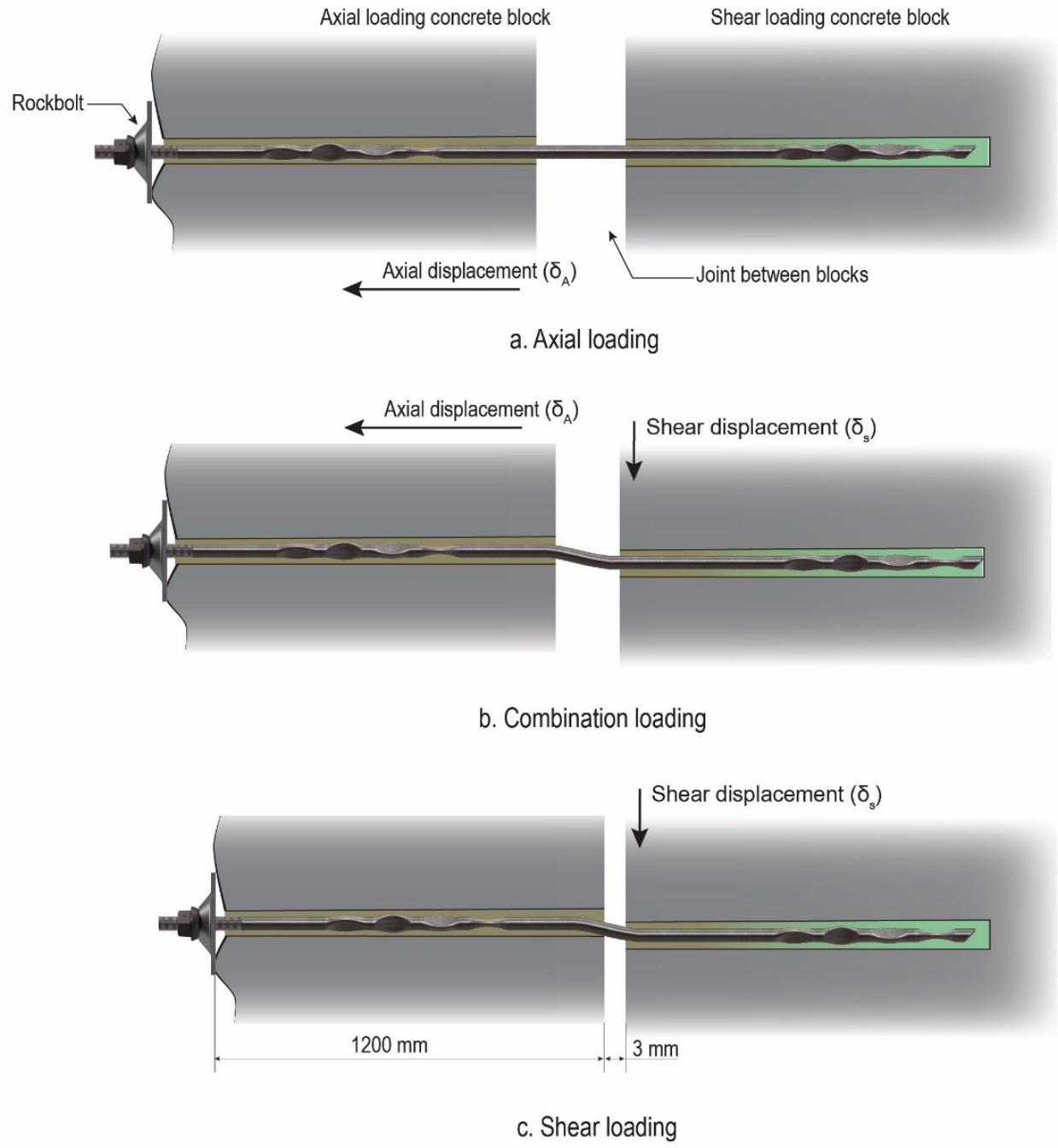


Figure 4 Illustration of loading cases. (a) Tensile loading (0°); (b) Combination loading (30 and 60°); (c) Shear loading (90°)

4 Presentation of results

4.1 Terminology

All laboratory results are presented as illustrated in Figure 5 and Table 1. $PE^{Q\alpha}$ is the quasi-static plastic energy dissipated during the loading cycle ('α' being the applied loading angle). This is different than the cumulative dissipated energy (PE_n^I) used to describe in analysing the results from impact tests (Hadjigeorgiou & Knox 2025).

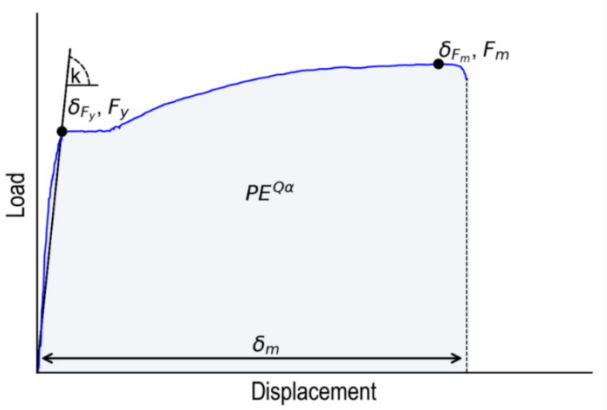


Figure 5 Load–displacement curve from quasi-static pull test. Displacement at yield load (δ_{Fy}), yield load (F_y), displacement at ultimate load (δ_{Fm}), ultimate load (F_m), and ultimate displacement (δ_m)

Table 1 Metrics used for presentation of results

Metric	Symbol	Unit	Definitions
Displacement loading angle	α	degrees	The resultant loading angle reference from the axial of the rockbolt
Displacement rate	$\dot{\delta}_X$	mm/s	The rate of displacement of a concrete block during loading $\dot{\delta}_A$ denotes the displacement rate of the axial concrete block and $\dot{\delta}_S$ denotes the displacement rate of the shear concert block
Stiffness	k	kN/mm	The gradient of the secant line through the point at which the rockbolt transitions from elastic to plastic deformation
Yield load	F_y	kN	The load at which the rockbolt transitions from elastic to plastic deformation
Displacement at yield load	$\delta_{F_y m}$	mm	The displacement at which the rockbolt transitions from elastic to plastic deformation
Ultimate load	F_m	kN	The maximum load recorded during the loading cycle
Maximum displacement	δ_m	mm	The maximum displacement recorded at the rupture of the rockbolt
Displacement at maximum load	δ_{F_m}	mm	The displacement at which the maximum load of the rockbolt is recorded
Quasi-static plastic energy dissipated	$PE^{Q\alpha}$	kJ	The plastic energy dissipated during the loading cycle. There 'α' denotes the applied loading angle

4.2 Influence of loading angle

The influence of the loading angle on the resulting load–displacement for the 3 rockbolt types is illustrated in Figure 6. All rockbolts displayed a large yielding displacement capacity at high loads justifying their characterisation as high energy absorption capacity rockbolts. A statistical summary of the experimental results are presented in Appendix A.

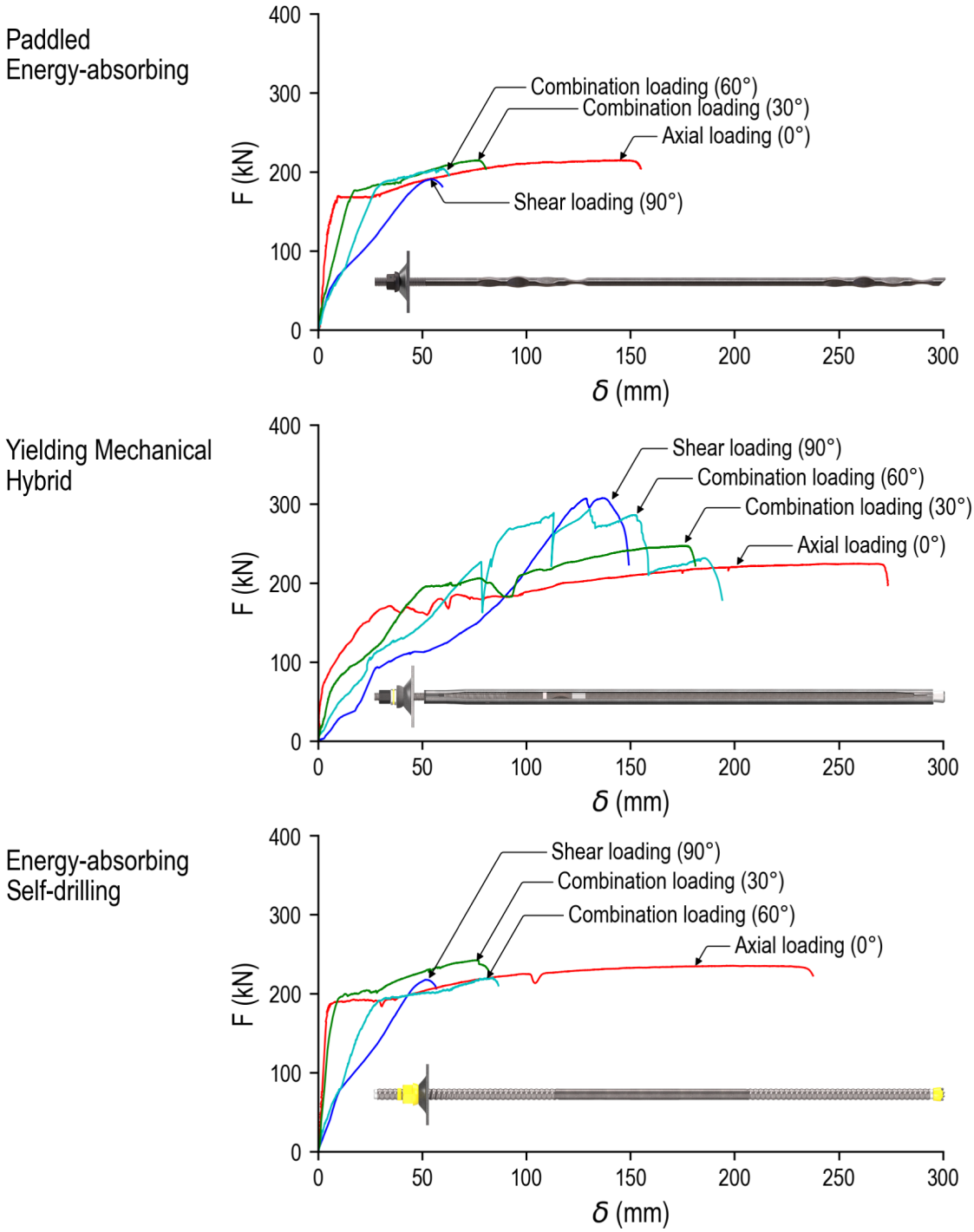


Figure 6 Load–displacement response to variations in loading angle in quasi-static pull tests

In response to an increase in the loading angle, both the PEAR and the energy-absorbing self-drilling rockbolt show a relative reduction in capacity. The YMHR response differs significantly when compared to the grouted energy-absorbing rockbolts. Although the shear load capacity is higher, the initial stiffness is lower at every loading angle. This is due to the mechanical anchor, which has a period of further mechanical activation during axial loading. In effect, the absence of a chemical encapsulation medium allows for additional lateral displacement prior to the activation of the reactive force of the friction unit and bar combination.

4.3 Influence of loading angle on the ultimate load capacity

A direct comparison of the ultimate load as a function of the loading angle is shown in Figure 7a and the influence of the loading angle on the relative ultimate load capacity in Figure 7b. In both cases, the dichotomy in response between the encapsulated and the YMHR is significant.

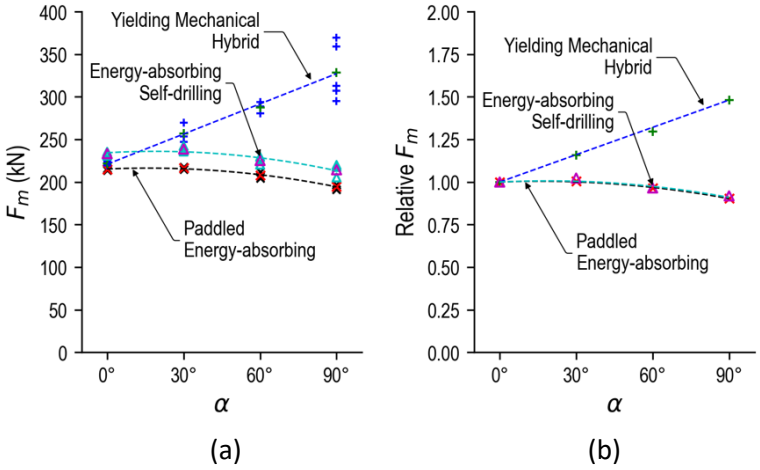


Figure 7 Influence of loading angle on (a) load capacity and (b) relative displacement

The PEAR and energy-absorbing self-drilling rockbolts displayed a minor increase in the load capacity (at 30° when compared to the load capacity recorded at 0°. Beyond 30°, the recorded load capacity decreased by less than 10% of the load capacity during the axial pull tests (α: 0°).

Of significance is the 50% increase in load capacity with an increase loading angle (α) for YMHR, which was not previously reported in the technical literature. The increase in capacity is due to the reinforcement mechanism of the YMHR whereby an increase in the loading angle results in greater contribution from the friction unit.

4.4 Influence of loading angle on displacement at ultimate load

All rockbolt types displayed an exponential decay in displacement as a function of an increase in the loading angle (α) (Figure 8). Although the rate of decay varied between rockbolt types a greater reduction in displacement occurred between 0 and 30°. This suggests that a minor component of shear loading (α < 30°) can result in a significant reduction in displacement capacity and consequently, the energy dissipation capacity of a rockbolt. This can explain variations in field performance of rockbolts subjected to inclined loading.

The impact of the shear loading component on the reduction in displacement was greater for the chemically encapsulated rockbolts. In YMHR the bar was able to displace in parallel to the surrounding friction unit. This resulted in a ‘softer’ response of the rockbolt as shearing of the tendon was induced at a greater displacement. Excluding the axial loading (α:0°) result, the greatest displacement recorded was at a loading angle (α) of 90° (i.e. pure shear).

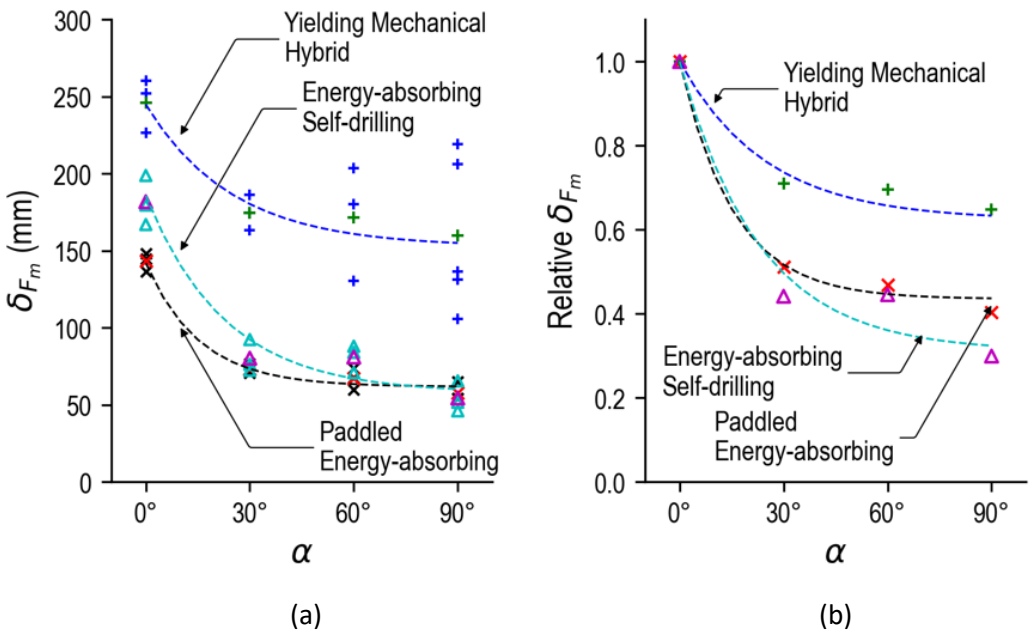


Figure 8 Influence of loading angle on displacement at ultimate load. (a) Absolute displacement at ultimate load capacity; (b) Relative displacement at ultimate load

4.5 Influence of loading angle on displacement at ultimate load

An exponential decay was observed in response to the increase in loading angle for both the PEAR and the energy-absorbing self-drilling rockbolt (Figure 9). A linear decrease in dissipated energy was observed for the YMHR, as the increase in load compensated for the decrease in displacement capacity.

The energy capacity of the YMHR was greater than that of the PEAR and energy-absorbing self-drilling rockbolt. This is defined by the difference in the length of mobilised steel between the anchor points and illustrated by the difference in the energy capacity.

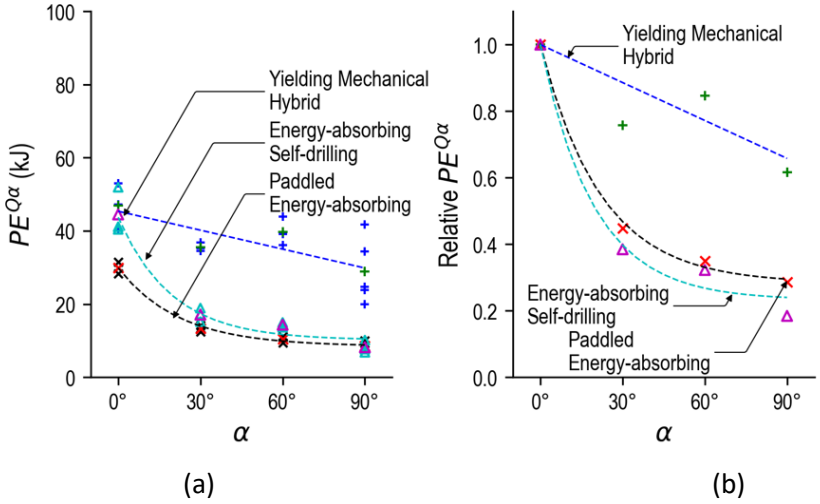


Figure 9 Influence of loading angle on the energy capacity of the rockbolts. (a) Absolute energy capacity; (b) Relative energy capacity

4.6 Visual examination of the rupture surface

An interpretation of the mechanical results was aided by visual observations of the rupture surfaces following each test. Figure 10 is a composite diagram that highlights the observed fracture mechanism under different loading angles for each rockbolt type.



Figure 10 Observed rupture mechanism under a range of loading angles for the different rockbolt types

A typical ductile tensile cup-and-cone rupture was observed at 0° for the PEAR. Tests at loading angles of 30, 60 and 90° resulted in an increase in the shear component, and a translation of the bar with respect to borehole in the direction of the motion of the shear block. The resulting translation of the bar and the fracturing of the chemical anchor and at all 3 loading angles may account for the 2-stage response observed in the load–displacement responses at 60 and 90°. While some borehole breakout of the concrete is observed at 30°, the volume of disturbed material increased at the loading angles of 60 and 90°.

As illustrated in Figure 10 at loading angles of 0° and 30° the tendon ruptured independently of the friction unit of the YMHR. The interface resistance between the friction unit and the borehole did not exceed the capacity of the material of the friction unit and the friction unit was sliding relative to the borehole. Both the friction unit and the tendon ruptured at loading angles of 60° and 90°. In addition, a greater breakout of the concrete surrounding the borehole was observed that in the 60° loading cases than the 90° loading angle.

In all energy-absorbing self-drilling rockbolt tests a typical cup-and-cone rupture interface in the axial loading (0°) case, transitioning to a shear interface and noticeable deformation of the hollow bar profile under shear loading (90°). Limited deviation from the original profile of the borehole was observed across all samples during the shear loading.

5 Conclusion

This paper discussed the full-scale response of the 3 rockbolt types under quasi-static combination loading. A comprehensive testing program investigated the effect of the loading configuration in relation to the

geometric features of the rockbolts. A critical factor in the response of the rockbolts to combination loading is the presence or absence of a chemical anchoring medium.

The YMHR was demonstrated to have superior shear capacity when compared to that of the PEAR and the energy-absorbing self-drilling rockbolt. An increase in load capacity (50%) and the least reduction in displacement capacity (35%) – in response to an increase in the quasi-static loading angle – was reported; however, a 'softer' initial stiffness and a greater variance was reported. When applying the YMHR in a ground support system, designers should recognise the potential for degradation due to corrosion and select an appropriate corrosion inhibitor.

The responses of the PEAR and the energy-absorbing self-drilling rockbolt to the combination were similar. A reduction in load capacity (≈10%) and an exponential decay in the displacement capacity was observed, with a primary component of the reduction occurring between 0 and 30°. For both the PEAR and the energy-absorbing self-drilling rockbolts, the final reduction in displacement capacity, at a loading angle of 90°, was greater than 59% relative to the displacement capacity under axial loading (0°).

The selection of a particular energy-absorbing rockbolt is a complex process that needs to account performance under a range of loading conditions, but also installation factors in difficult ground conditions, as well as long-term performance in potentially corrosive environments.

Acknowledgement

The authors would like to acknowledge the Natural Science and Engineering Research Council of Canada and Epiroc for providing access to the testing facilities.

Appendix

Table 2 Effect of loading angle on the ultimate load for the 3 different rockbolt types

Rockbolt	Loading angle (α) (˚)	Min F_m (kN)	Max F_m (kN)	Avg F_m (kN)	SD	CV %
Paddled energy-absorbing rockbolt	0	214	216	215	1.1	0.5
	30	215	218	216	1.6	0.7
	60	204	212	208	3.7	1.8
	90	191	197	195	3.2	1.6
Yielding mechanical hybrid rockbolt	0	220	224	222	2.4	1.1
	30	247	270	257	11.5	4.5
	60	281	294	288	6.6	2.3
	90	295	370	329	33.3	10.1
Energy-absorbing self-drilling rockbolt	0	231	235	233	2.2	1.0
	30	236	242	239	3.3	1.4
	60	220	230	225	4.6	2.0
	90	205	220	214	7.9	3.7

Table 3 Effect of loading angle on displacement at ultimate load for the three 3 rockbolt types

Rockbolt	Loading angle (α) (˚)	Min δ_{Fm} (mm)	Max δ_{Fm} (mm)	Avg δ_{Fm} (mm)	SD	CV %
Paddled energy-absorbing Rockbolt	0	137	148	143	6.0	0.5
	30	71	77	73	3.0	4.2
	60	60	74	67	7.0	10.5
	90	54	65	58	6.3	10.9
Yielding mechanical hybrid rockbolt	0	226	260	246	17.7	7.2
	30	163	186	175	11.6	6.6
	60	130	204	171	37.4	21.8
	90	106	219	160	49.9	31.3
Energy-absorbing self-drilling rockbolt	0	167	199	182	16.0	8.8
	30	72	92	80	10.6	13.2
	60	71	88	81	9.0	11.1
	90	46	66	54	10.0	18.4

Table 4 Effect of loading angle on energy capacity for the 3 different rockbolt types

Rockbolt	Loading angle (α) (˚)	Min $PE^{Q\alpha}$ (kJ)	Max $PE^{Q\alpha}$ (kJ)	Avg $PE^{Q\alpha}$ (kJ)	SD	CV %
Paddled energy-absorbing rockbolt	0	28	31	30	1.6	5.3
	30	12	14	13	0.9	6.9
	60	9	11	10	0.9	8.8
	90	7	10	9	1.3	15.0
Yielding mechanical hybrid rockbolt	0	40	53	47	6.4	13.5
	30	35	37	36	1.2	3.3
	60	36	44	40	3.9	9.9
	90	20	42	29	8.9	30.9
Energy-absorbing self-drilling rockbolt	0	40	52	44	6.4	14.5
	30	15	19	17	1.9	10.9
	60	14	15	14	0.7	4.6
	90	7	10	8	1.7	21.1

References

Chen, Y & Li, CC 2015, 'Performance of fully encapsulated rebar bolts and D-Bolts under combined pull-and-shear loading', *Tunnelling and Underground Space Technology*, vol. 45, pp. 99–106.

Hadjigeorgiou, J & Knox, G 2025, 'Interpreting energy-absorption values for rockbolts from quasi static and impact tests', *ISRM International Symposium Eurock 2025 – Expanding the Underground Space,* Trondheim.

Knox, G & Hadjigeorgiou, J 2022, 'Influence of testing configuration on the performance of paddled energy-absorbing rockbolts under impact loading', *Rock Mechanics and Rock Engineering*, vol. 55, pp. 5705–5721.

Knox, G & Hadjigeorgiou, J 2023a, 'Performance in shear of mechanical hybrid rockbolts', in J Wesseloo (ed.), *Ground Support 2023: Proceedings of the 10th International Conference on Ground Support in Mining*, Australian Centre for Geomechanics, Perth, pp. 495–506, https://doi.org/10.36487/ACG_repo/2325_33

Knox, G & Hadjigeorgiou, J 2023b, 'Performance of conventional and energy-absorbing self-drilling hollow core rockbolts under controlled laboratory conditions', *Rock Mechanics and Rock Engineering*, vol. 56, pp. 4363–4378.

Knox, G & Hadjigeorgiou, J 2024a, 'Behaviour of paddled energy-absorbing rockbolts under complex loading laboratory conditions.' *Journal of the Southern African Institute of Mining and Metallurgy*, vol. 124, no. 9. pp. 535–546.

Knox, G & Hadjigeorgiou, J 2024b, 'Behaviour of yielding mechanical hybrid rockbolts under complex loading conditions' *International Journal of Rock Mechanics and Mining Sciences*, vol. 182.

Knox, G & Hadjigeorgiou, J 2025, 'Rockbolts in shear', *Journal of the Southern African Institute of Mining and Metallurgy*, vol. 125, no. 11. pp. 621–628.

Li, C 2010, 'A new energy-absorbing bolt for rock support in high stress rock masses', *International Journal of Rock Mechanics and Mining Science*, vol. 47, pp. 396–404.

Li, CC, Hadjigeorgiou, J, Mikula, P, Knox, G, Darlington, B, Royer, R & Hosp M, 2021, 'Performance of Identical rockbolts tested on four dynamic testing rigs employing the direct impact method', *Journal of Rock Mechanics and Geotechnical Engineering*, vol. 13, no. 4, pp. 745–754.